J Nanopart Res (2017) 19: 103
DOI 10.1007/s11051-017-3769-y

RESEARCH PAPER

# Generation and thermally adjustable catalysis of silver nanoparticle immobilized temperature-sensitive nanocomposite

**Jun Xu · Tao Zhou · Lei Jia · Xiaoke Shen · Xiaohui Li · Huijun Li · Zhouqing Xu · Jianliang Cao**

Received: 30 October 2016 / Accepted: 24 January 2017 / Published online: 10 March 2017


**Abstract** The rise in environmental issues due to the catalytic degradation of pollutants in water has received much attention. In this report, a facile method was developed for the generation of a novel thermosensitive Ag-decorated catalyst, $SiO_2$@PNIPAM@Ag (the average particle size is around 540 nm), through atom transfer radical polymerization (ATRP) and mild reducing reactions. First, poly(N-isopropylacrylamide) (PNIPAM) was used to create a shell around mercapto-silica spheres that allowed for enhanced catalyst support dispersion into water. Second, through a mild reducing reaction, these Ag nanoparticles (NPs) were then anchored to the surface of $SiO_2$@PNIPAM spheres. The resulting catalyst revealed catalytic activity to degrade various nitrobenzenes and organic dyes in an aqueous solution with sodium borohydride ($NaBH_4$) at ambient temperature. The catalytic activity can be adjusted in different temperatures through the aggregation or dispersion of Ag catalyst on the polymer supporters, which is due to the thermosensitive PNIPAM shell. The ease of preparation and efficient catalytic activity of the catalyst can make it a promising candidate for the use in degrading organic pollutants for environmental remediation.

J. Xu · T. Zhou · L. Jia (✉) · X. Shen · X. Li · H. Li · Z. Xu · J. Cao (✉)
College of Chemistry and Chemical Engineering, Henan Polytechnic University, Jiaozuo 454000, China
e-mail: jlxj@hpu.edu.cn
e-mail: caojianliang@hpu.edu.cn

**Keywords** Silver nanoparticle · Catalyst · Core-shell structure · Thermosensitivity · Sensors

## Introduction

Due to rapid international industrial and societal development, water pollution has become one of the predominant environmental problems (Sun et al. 2014). These pollutants include 4-nitrophenol (4-NP) and its derivatives, which are used frequently to make fungicides, insecticides, herbicides, pesticides, rubbers, and synthetic dyes (Liu et al. 2007). Because of their high solubility and stability, these chemicals are particularly worrisome pollutants in natural water and wastewater systems (Sugiyama et al. 2012). Furthermore, the toxicity of 4-NP is higher than that of other phenol derivatives (Sugiyama et al. 2012), particularly for green plants and for aquatic organisms found in surface waters, where high levels of toxicity occur even at trace amounts (Ehlerovaa et al. 2008). Therefore, removal of 4-NP from water is a priority. One method of removal is conversion to 4-aminophenol (4-AP), which has lower levels of toxicity and higher biodegradability in the environment (Batzli and Love 2015). Additionally, 4-AP is an important industrial intermediate used in manufacturing of anticorrosion lubricants, corrosion inhibitors, and pharmaceuticals (Uberoi and Bhattacharya 1997; Swathi and Buvaneswari 2008). Therefore, the 4-AP resulting from reduction of 4-NP

would not only promote environmental detoxification but also contribute to the demand for manufacturing chemicals. Furthermore, the degradation of 4-NP into 4-AP has been the focus of a number of studies and has served as a model reaction when studying the catalytic activity of a range of nanoparticles because it incurs no byproducts and is able to be monitored by UV-Vis spectroscopy (Naik et al. 2011; Li et al. 2015a, b; Gao et al. 2015).

Due to their unusual chemical and physical attributes, metal NPs exhibit high catalytic activity compared to bulk materials and thus are capable of catalyzing a number of chemical reactions, especially those involving reduction-oxidation (redox) (Mu et al. 2014; Zhang et al. 2012; Zhang et al. 2014; Peng et al. 2008). Along these lines, nanocomposites coated with Ag have recently received considerable attention due to an ability to degrade organic pollutants, methyl orange (Tang et al. 2013), methylene blue (Sohrabnezhad et al. 2014), rhodamine B (Li et al. 2013), and 4-NP (Zheng et al. 2015).

However, compared with metal ions, although metal NPs can significantly affect the catalytic activity in varying dimensions, the agglomeration of metal NPs due to high surface energy and Van der Waals forces is inevitable (Medasani et al. 2007; Lee et al. 2008). In order to solve the problem about NPs aggregation, many techniques have been developed, such as stabilizing NPs by surfactants (Li et al. 2015a, b; Khanna et al. 2007; Boutros et al. 2008; Deng et al. 2012) or dispersing NPs on the structural supports (Ravula et al. 2015; Jia et al. 2012; Zhang et al. 2012; Wang et al. 2013). Among various measures, the preparation of polymer colloidal matrix through radical polymerization was an ideal method, which can play a role as surfactant to avoid aggregation of metallic NPs (Lu et al. 2006). Based on the idea mentioned above, various functional polymers with thermosensitivity have been used as catalyst supporter for metal NPs to adjust the catalytic behavior by a thermodynamic transition (Chen et al. 2014; Zetterlund et al. 2008; Monteiro and Cunningham 2012; Liu et al. 2015; Contreras-Cáceres et al. 2008; Wu et al. 2012). Poly(N-isopropylacrylamide) (PNIPAM) have been widely investigated due to the volume phase transition in aqueous media, and its invertible collapse/swelling transition around the lower critical solution temperature (LCST, about 32 °C) (Fujishige et al. 1989; Wei et al. 2009; Liu et al. 2013). Thus, the research of PNIPAM-based microgels have received many attentions in the area of drug delivery (Bysell et al. 2011), bioseparation (Matsuzaka et al. 2013), and catalysis (Contreras-Cáceres et al. 2008).

Consequently, a simple and soft chemical polymerization route is presented for synthesizing Ag-decorated $SiO_2$@PNIPAM core-shell composite microgels ($SiO_2$@PNIPAM@Ag). A diagram of the preparation is displayed in Fig. 1. The fabrication of uniform Ag NP-loaded $SiO_2$@PNIPAM microgel shell was successfully accomplished, which can prevent the aggregation of Ag NPs. Furthermore, the existence state (collapse or tumidness) of PNIPAM shell can change with reaction temperature as a steerable Ag controller, which can adjust catalytic activity to the best state near room temperature. The results indicated that the $SiO_2$@PNIPAM@Ag catalyst exhibited excellent catalytic performance for the reduction of nitrobenzene and organic dyes, and the catalytic properties of the catalyst could be adjusted accordingly with the thermosensitivity of the composite microgel template. Our present constructed $SiO_2$@PNIPAM@Ag catalyst not only achieved the efficient catalysis but also focused on the idea of intelligent catalysis, which can solve pollution problems near optimal environmental temperature. Moreover, the reported strategy on the fabrication of Ag NPs trapped into thermosensitive polymers can provide some useful information in design of other functional materials related to green and efficient catalysts.

## Experimental methods

### Materials

3-Mercaptopropyl trimethoxysilane (MPTMS), 2-bromo-2-methylpropionyl bromide, N-isopropylacrylamide (NIPAM), and N,N,N′,N′,N′-pentamethyldiethylenetriamine (PMDETA) were purchased from Aldrich. 4-nitrophenol, 2,4-dinitroaniline, $AgNO_3$, $NaBH_4$, zinc powders, trisodium citrate, and CuBr were obtained from the Shanghai Chemical Reagent Co., China. THF and other solvents were of analytical grade from Beijing Chemical Factory (China) and were used without further purification.

### Preparation of $SiO_2$-Br

The initiator 2-bromopropionyl bromide was loaded onto silica surface through chemical reactions in the presence of zinc powders. A certain volume of 2-bromopropionyl bromide solution (0.1 mL) was

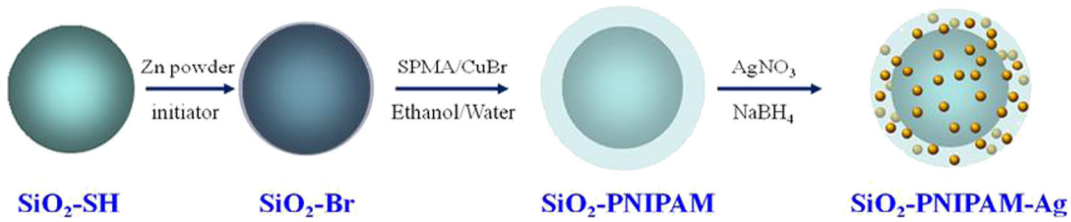


**Fig. 1** The schematic illustration for the preparation of $SiO_2$@PNIPAM@Ag catalyst

slowly added to the suspension of $SiO_2$-SH (500 mg) and zinc powders (100 mg) in anhydrous THF (50 mL); the mixture was then stirred for 24 h. Finally, the $SiO_2$-Br spheres were collected by centrifugation and washed with THF, diluted hydrochloric acid, and deionized water three times before dried in oven.

### Preparation of $SiO_2$@PNIPAM by ATRP

Anchorage of PNIPAM shells on the surface of Ag NPs was carried out at RT (Li et al. 2007). Briefly, the mixed solution containing $SiO_2$-Br (about 580 mg), NIPAM (1.358 g, 12 mmol), and CuBr (21.45 mg, 0.15 mmol) was degassed with $N_2$ for several cycles. Then, the reaction was started by adding another degassed mixture including PMDETA (78.16 mg, 0.45 mmol) and 2-propanol/water (1:1, 3 mL) into the above solution and reacted for 3 h in $N_2$ atmosphere. Finally, the $SiO_2$@PNIPAM were collected by centrifugation and washed with deionized water three times and the product was then redistributed in deionized water.

### Preparation of $SiO_2$@PNIPAM@Ag spheres

The existing $SiO_2$@PNIPAM (500 mg) was first dispersed in 100-mL deionized water, and the pH of the solution was adjusted to 10 by addition of certain amounts of dilute solution at 85 °C. After stirring for 1 h, 1.6 mL of $AgNO_3$ aqueous solution (0.35 M) was added to the above solution and the mixture was stirred for another 1 h. In order to reduce $Ag^+$ adsorbed by PNIPAM, 50 mL of ethanol and 1-mL trisodium citrate solution (0.36 M) were added, after gently stirring for half an hour, the $Ag^+$ can be reduced to Ag. The finally products were collected by centrifugation and washed with deionized water three times and then redistributed in deionized water.

### Catalytic reduction of nitrobenzene

The reduction of 4-nitrophenol with $NaBH_4$ was carried out to examine the catalytic activity and reusability of the $SiO_2$@PNIPAM@Ag catalyst. Amounts of 2 mL of deionized water, 0.25 mL of 4-NP aqueous solution ($3.4 \times 10^{-3}$ M), and 0.25 mL of fresh $NaBH_4$ (1.2 M) were added into the bottle in batch, followed by addition of 0.12 mL of catalyst (1 mg $mL^{-1}$ ). During the reaction, the absorbance of solution was recorded by the UV–Vis spectrophotometer. After the whole reduction process was completed, the catalysts were separated by centrifugation and the recycling experimental condition was the same as above.

## Characterization

Transmission electron microscopy (TEM) was performed at acceleration voltages of 200 and 300 kV with a JEOL 2100FX and Tecnai-G2-F30. A single drop of testing sample was added onto the surface of TEM grid, and the solvent was allowed to evaporate. The sample was then characterized by TEM without further modification. X-ray diffraction (XRD) measurements were carried out on a X'pert PRO X-ray power diffractometer using Cu Ka radiation of 1.5406 A (40 kV, 30 mA). The KBr pressed disk method was used to obtain IR spectra ($\nu$ = 4000–400 $cm^{-1}$) via a Bruker V70 FT-IR spectrophotometer.

## Results and discussion

### Structure and composition analysis of the composite microgels

First, mercapto-silica spheres were generated using a previously described method (Lu et al. 2011). To

prepare the initiator modified $SiO_2$-Br spheres, the mercapto-silica spheres were combined with zinc powders and 2-bromopropionyl bromide at room temperature. The resulting NPs were then coated with a PNIPAM shell of a specified thickness using atom transfer radical polymerization (ATRP) process. The TEM image presented in Fig. 2a demonstrated the original silica spheres were approximately 541.19 ± 5.68 nm in size and had a high degree of monodispersity. The accurate control of appropriate reaction conditions during the ATRP process generated an observable external polymer shell on the mercapto-silica spheres (as shown in Fig. 2b), suggesting successful grafting. Furthermore, the generated spheres displayed increased dispersion in room-temperature water compared to the original silica spheres, which can be attributed to the solubilizing nature of PNIPAM. The obtained FT-IR was also consistent with chemical linkage between $SiO_2$-SH and PNIPAM. Two peaks characteristic of PNIPAM at 1653 and 1550 $cm^{-1}$, which are indicative of amine and N–H stretches, respectively (You et al. 2008), were noted for $SiO_2$@PNIPAM (Fig. 3a). In addition, the wide peaks at 2980–2860 $cm^{-1}$ can be attributed to the vibration of C–H bonds in PNIPAM chains. Finally, a mild reaction was performed to attach Ag NPs to the $SiO_2$@PNIPAM sphere surfaces.

On the basis of effective reduction method and the evident TEM contrast between NPs and silica spheres, we supposed that the surface-attached $SiO_2$@PNIPAM spheres were composed of Ag NPs. The data in Fig. 2c supported the in situ anchoring of Ag-NPs, which were uniformly distributed on $SiO_2$@PNIPAM without obvious aggregation. Such a Ag-NP-decorated $SiO_2$@PNIPAM structure can be further confirmed with the corresponding HRTEM analyses, which was shown in Fig. 2d. The close-up observation of Fig. 2d indicated that the vast majority of Ag NPs with grain diameters in the range of 15–20 nm. The lattice fringe spacing of the obtained Ag NPs is 0.242 and 0.208 nm, which can be clearly assigned to the (111) and (200) planes of *fcc* Ag.

The formation of $SiO_2$@PNIPAM@Ag spheres was further supported by XRD analysis, which displayed the characteristic broad diffraction peaks of silica spheres (Fig. 3b). Following polymerization and in situ reduction, the diffraction peaks of $Ag^0$ fell at 2θ = 38.116° (d = 0.2120 nm, 111 plane), 44.277° (d = 0.2446 nm, 200 plane), 64.426° (d = 0.3460 nm, 220 plane), and 77.472° (d = 0.4062 nm, 311 plane) (Liu et al. 2012)

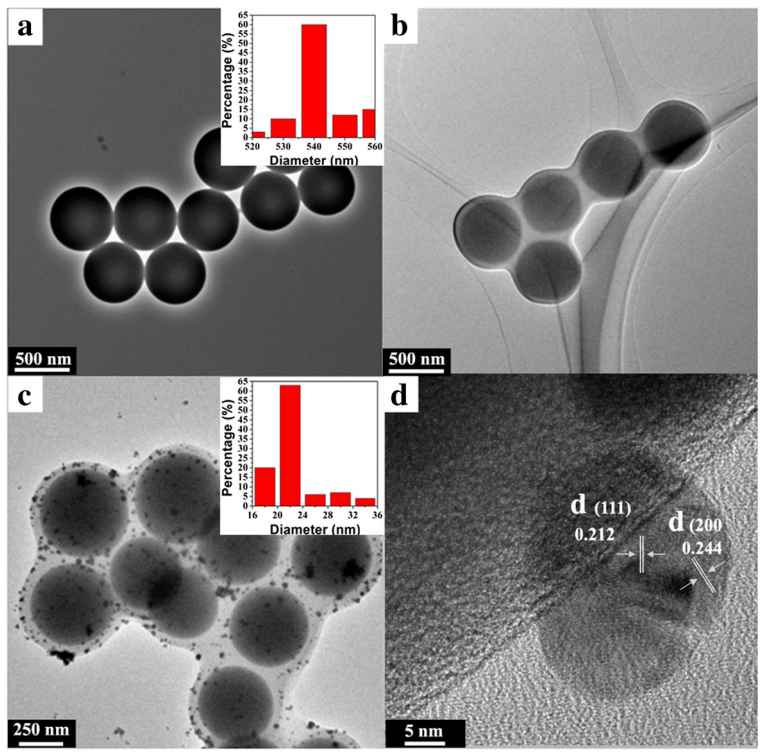


**Fig. 2** TEM images of the original $SiO_2$-SH (**a**), $SiO_2$-PNIPAM (**b**), $SiO_2$-PNIPAM-Ag (**c**), and the high resolution of the the Ag NP in the edge of the $SiO_2$-PNIPAM-Ag spheres (**d**). *Inset images* in the *top right corner* of **a** and **c** are the size distribution histograms of $SiO_2$-SH spheres and Ag NPs

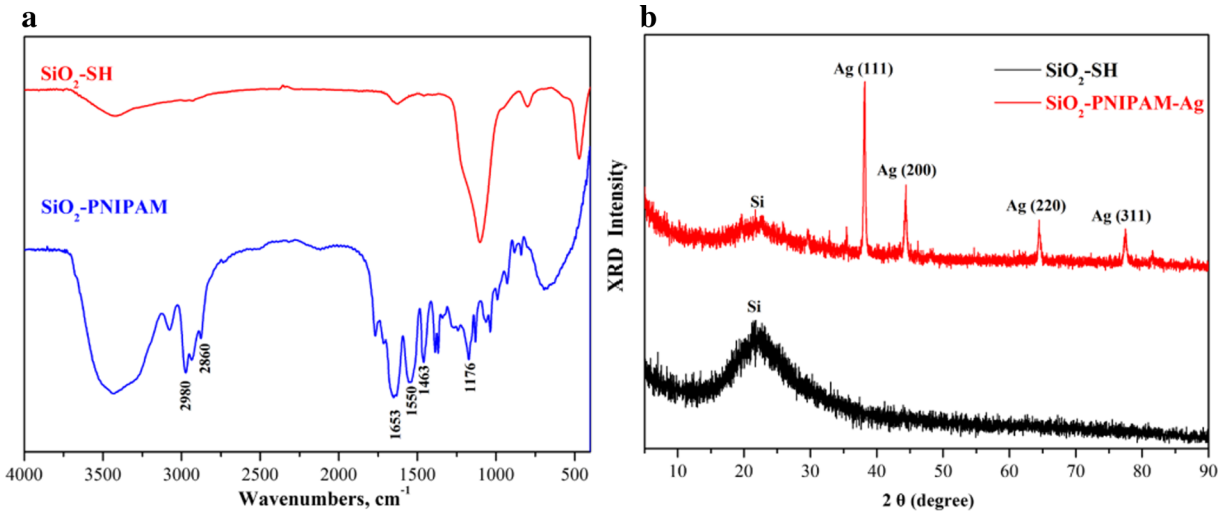


**Fig. 3** **a** Infrared spectroscopy of the $SiO_2$@PNIPAM spheres; **b** XRD patterns for pristine $SiO_2$-SH and $SiO_2$@PNIPAM@Ag NSs

(JCPDS 65–2871), indicating successful deposition of Ag NPs. Meanwhile, no significant changes were noted in the wide diffraction peaks of the silica spheres, supporting the preservation of the silica sphere structures during reduction.

## Catalytic activity for the reduction of various nitrobenzenes and dyes

The excellent catalytic abilities and selectivity of Ag NPs in a number of reactions such as reduction of 4-NP have been long documented (Xie et al. 2014; Lee and Jang 2016). In this work, we investigated the catalytic activity of $SiO_2$@PNIPAM@Ag catalyst as the change of temperature in the reduction of 4-NP. Importantly, Ag-NP immobilization onto $SiO_2$@PNIPAM endowed the composite with satisfactory catalytic activity, while this reaction failed to occur even over a period of more than 2 days in the absence of $SiO_2$@PNIPAM@Ag catalyst. As shown in Fig. 4a, b, the $SiO_2$@PNIPAM@Ag catalyst demonstrated excellent catalytic activity at 25 and 45 °C, respectively. With the extension of time, the peak at 400 nm of 4-NP was continuously reduced with a corresponding decline in their absorption peaks in the ultraviolet spectrum. The new peak appearing at 300 nm was normally ascribed to the formation of the catalytic product 4-AP. Additionally, the Ag plasmon bands that approximate 410 nm were not observed in the UV–Vis absorbance spectra of the solution of the two substrates following catalytic reduction by $NaBH_4$. This indicated that Ag-NPs were stably anchored on the $SiO_2$@PNIPAM surfaces, and no detachment occurred. It is worth noting that the catalytic efficiency was seemingly higher under the relatively low temperature (25 °C), while the higher temperature caused depressed catalytic efficiency (45 °C), which indicated an abnormal catalytic behavior.

To compare the catalytic efficiency of the $SiO_2$@PNIPAM@Ag spheres under different temperature quantitatively, a kinetic rate constant $k$ was calculated and used to evaluate each catalytic system. The pseudo-first-order kinetics are often described as $\ln(C_t/C_0) = -kt$, where $C_t$ is the concentration of substrates at time $t$, $C_0$ is the original concentration of substrates, and $k$ is the degradation rate (Zhu et al. 2013). The catalytic results follow pseudo-first-order kinetics as indicated by the linear relationship of $C_t/C_0$ and $\ln(C_t/C_0)$ versus time ($t$) for the $SiO_2$@PNIPAM@Ag catalyst, as shown in Fig. 4c, d. The rate constants were estimated from the slope of a linear fit in the plots as 0.247 and 0.085 $min^{-1}$ for 4-NP at 25 and 45 °C, respectively. This suggests that the $SiO_2$@PNIPAM@Ag spheres had significantly higher catalytic activity for the reduction of 4-NP below the lower critical solution temperature of PNIPAM chains(Liu et al. 2013, 2015). Furthermore, we can see that the reduction had good linear relations at all tested temperatures, which indicated that this catalytic reaction agrees with the pseudo-first-order kinetics. Although the reduction of 4-NP were carried out very smoothly under various temperature, the slopes shown in Fig. 4d were highly affected by the temperature. The reaction displayed increasing rate constant when the temperature is below 35 °C, while the rate constant decreased when the temperature is above 35 °C. However, when the reaction temperature is higher than 45 °C, the rate

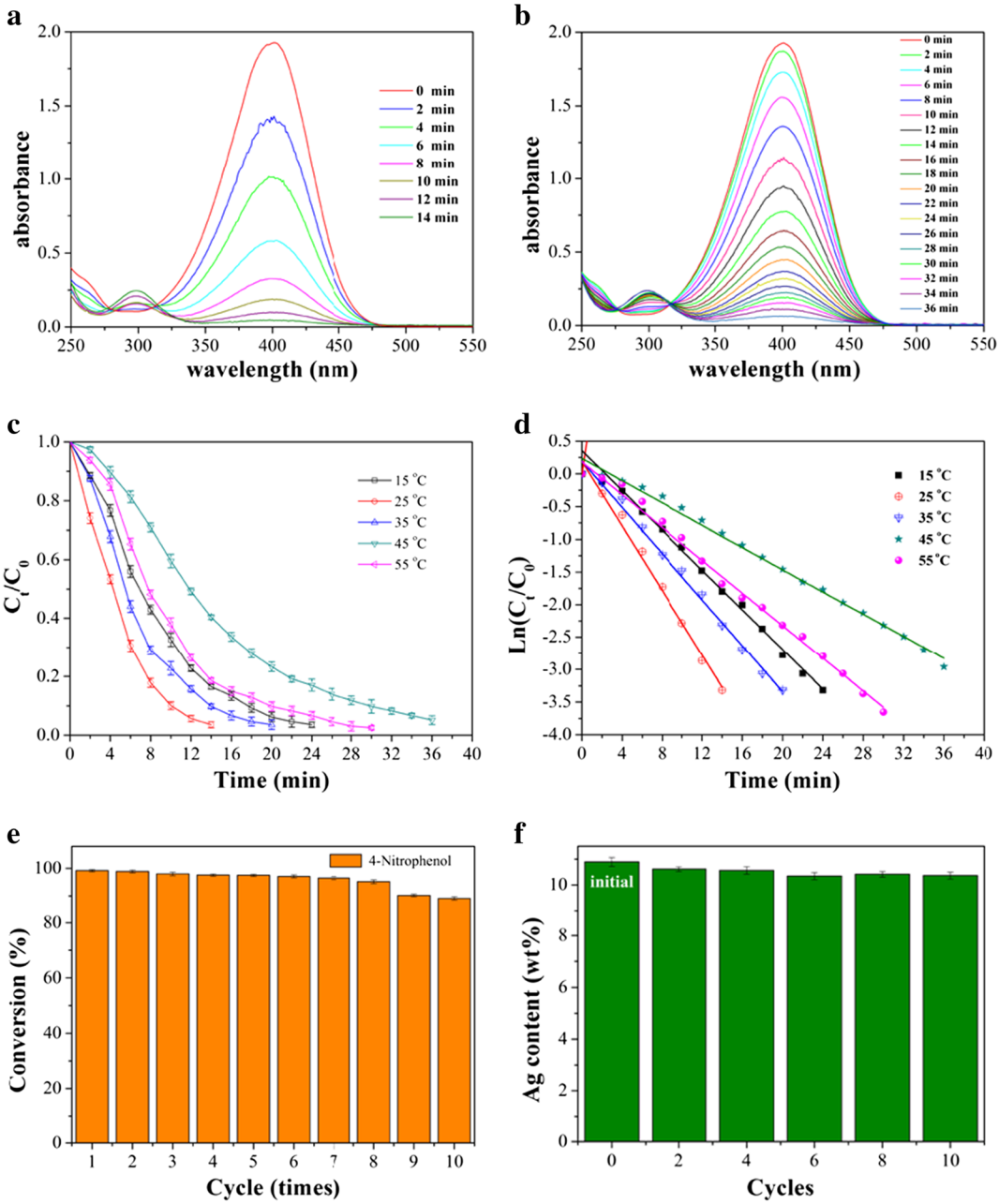


**Fig. 4** Successive *UV–vis* absorption spectra of the reduction of 4-nitrophenol at 25 °C (**a**) and 45 °C (**b**) catalyzed by $SiO_2$@PNIPAM@Ag. The plots of Ct/C0 (**c**) and Ln(Ct/C0) (**d**) versus the time *t* at different temperature. **e** Catalytic conversions of 4-NP for ten successive cycles with the same batch of $SiO_2$@PNIPAM@Ag spheres. **f** changes of Ag content after each 2 cycles

constant increased again. We speculated that the elastic catalytic rate may be caused by the thermosensitive property of PNIPAM chains, mainly shown in the following aspects. When the reaction temperature is below the LCST, the PNIPAM chains are in a stretching state, which can lead the expansion of the Ag NPs and increase the contact with 4-NP. In this case, the catalytic rate only depended on the thermoactivity, so the rate constant increased with temperature. When the reaction temperature is around the LCST, the continuous shrinking of the PNIPAM network will occur and reduce the exposure of Ag NPs and 4-NP. The polymer shell

changed from hydrophilic to hydrophobic and thus led to the reduction of the catalytic rate. When the reaction temperature is above the LCST, additional shrinking of the PNIPAM network will continue to happen and the rate constant rises again as the temperature increases. However, there is no additional shrinking of the PNIPAM network when the temperature is higher than 45 °C, which resulted in the continuous increase of the reaction rates with temperature.

Furthermore, the catalytic activity of the $SiO_2$@PNIPAM@Ag catalyst for the reduction of other nitrobenzene analogs including nitroaniline, nitrotoluene, and organic dyes (Table 1) were also investigated. All the catalytic conditions of these substrates are the same as 4-NP, and the conversion was determined by the gas chromatography/mass spectroscopy (GC/MS) analysis after reaction. As shown in Table 1, the $SiO_2$@PNIPAM@Ag catalyst exhibited good catalytic activity for the above substrates regardless of the types and position of the substituents. Four kinds of nitroaniline analogs and two kinds of organic dyes can be transformed within 13 min with a conversion greater than 95%. While for the nitrotoluene analogs, the $SiO_2$@PNIPAM@Ag catalyst displayed low catalytic activity and the reaction time obviously extended. The possible reason for this phenomenon is that the reaction processes of nitrotoluene analogs are more complicated, which can produce amino and nitroso-type products while nitroaniline and nitrophenol can only be converted into corresponding anilines (Dotzauer et al. 2009).

Importantly, the prepared catalyst displayed excellent reusability when tested for 10 cycles (Fig. 4e). Overall, even if the initial reduction rate decreased with the increasing of the number of cycles, especially after more than 6 cycles, the efficiency of the final catalysis had no reduction, which was confirmed by the Ag content after each 2 cycles (Fig. 4f). More than 80% of Ag content was maintained on catalyst even after ten runs, which proved the $SiO_2$@PNIPAM@Ag catalyst displayed potential as a reusable catalyst.

## Conclusions

The generation of novel materials by adopting new methods plays a vital role in academic and industrial fields. In this present work, well-defined core–shell

**Table 1** Reduction of various nitrobenzenes and dyes at 25 °C using $SiO_2$-PNIPAM-Ag catalyst[a]

| Entry | Compound | Structure | Time/min | Conversion |
|---|---|---|---|---|
| 1 | p-Nitroaniline |  | 6 | 99 |
| 2 | m-Nitroaniline |  | 9 | 99 |
| 3 | o-Nitroaniline |  | 8 | 99 |
| 4 | 2,4-Dinitroaniline |  | 9 | 99 |
| 5 | 2,4-Dinitrotoluene |  | 105 | 82 |
| 6 | m-Nitrotoluene |  | 120 | 85 |
| 7 | o-Nitrotoluene |  | 118 | 83 |
| 8 | Congored | 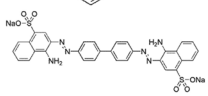 | 12 | 96 |
| 9 | Methylene | 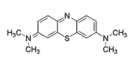 | 13 | 95 |

[a] Reaction condition: 0.25 mL of $3.4 \times 10^{-3}$ M substrates, 0.06 mL of 1 mg $mL^{-1}$ catalyst, and 0.25 mL of 1.2 M fresh $NaBH_4$

structured polymer/inorganic hybrid composite consisting of a $SiO_2$ core coated with a shell of PNIPAM–Ag were synthesized using ATRP and a mild reducing reaction. The solubilizing properties of PNIPAM resulted in improved dispersion of the resultant spheres in water. The synthesized $SiO_2$@PNIPAM@Ag catalyst displayed high catalytic activity and excellent recyclability when reducing various nitrobenzenes and dyes. Importantly, the catalytic activity of $SiO_2$@PNIPAM@Ag catalyst can be regulated by collapse/swelling of PNIPAM network, which led to the aggregation or dispersion of Ag NPs. In addition, the catalytic system can be recycled efficiently after 10 cycles, and most of the Ag NPs were still maintained on catalyst. This simple method may extend to the preparation of other catalysts with the potential for other practical applications such as water purification, selective catalysis, sensing devices, and green chemistry.

4-NP, 4-nitrophenol; 4-AP, 4-aminophenol; ATRP, atom transfer radical polymerization; GC/MS, gas chromatography/mass spectroscopy; LCST, lower critical solution temperature; MPTMS, 3-mercaptopropyl trimethoxysilane; $NaBH_4$, sodium borohydride; NIPAM, *N*-isopropylacrylamide; NPs, nanoparticles; PMDETA, *N*,*N*′,*N*′,*N*′,*N*″-pentamethyldiethylenetriamine; PNIPAM, poly(*N*-isopropylacrylamide); TEM, transmission electron microscopy; XRD, X-ray diffraction.

#### Compliance with ethical standards

**Funding** This work was supported, in part, by the National Natural Science Foundation of China (Nos. 21404033, 21401046, and 51404097), the Technology Research Project of Henan province (162102210065 and 152102210314), the Program for Science and Technology Innovation Talents in Universities of Henan Province (17HASTIT029), and the Foundation for Distinguished Young Scientists of Henan Polytechnic University (J2016-2).

**Conflict of interest** The authors declare that they have no conflict of interest.

## References

Batzli KM, Love BJ (2015) Formation of platinum-coated templates of insulin nanowires used in reducing 4-nitrophenol. Mater Sci Eng C-Mater 48:103–111

Boutros M, Denicourt-Nowicki A, Roucoux A, Gengembre L, Beaunier P, Gédéon A, Launay F (2008) A surfactant-assisted preparation of well dispersed rhodium nanoparticles within the mesopores of AlSBA-15: characterization and use in catalysis. Chem Commun 25:2920–2922

Bysell H, Mansson R, Hansson P, Malmsten M (2011) Microgels and microcapsules in peptide and protein drug delivery. Adv Drug Deliv Rev 63:1172–1185

Chen J, Xiao P, Gu J, Han D, Zhang J, Sun A, Wang W, Chen T (2014) A smart hybrid system of Au nanoparticle immobilized PDMAEMA brushes for thermally adjustable catalysis. Chem Commun 50:1212–1214

Contreras-Cáceres R, Sánchez-Iglesias A, Karg M, Pastoriza-Santos I, Pérez-Juste J, Pacifico J, Hellweg T, Fernández-Barbero A, Liz-Marzán LM (2008) Calculation of annual abundance indices for bigeye tuna in the Indian Ocean using Japanese longline catch and effort data. Adv Mater 20:1666–1670

Deng Z, Zhu H, Peng B, Chen H, Sun Y, Gang X, Jin P, Wang J (2012) Synthesis of PS/Ag nanocomposite spheres with catalytic and antibacterial activities. ACS Appl Mater Interfaces 4:5625–5632

Dotzauer DM, Bhattacharjee S, Wen Y, Bruening ML (2009) Nanoparticle-containing membranes for the catalytic reduction of nitroaromatic compounds. Langmuir 25:1865–1871

Ehlerovaa J, Trevanib L, Sedlbauera J, Ballerat-Busserollesc K, Tremaineb PR (2008) UV–visible spectroscopic study on nitrophenols ionization reactions to 225 °C. Proceedings of the 15th International Conference on the Properties of Water and Steam

Fujishige S, Kubota K, Ando I (1989) Phase transition of aqueous solutions of poly(N-isopropylacrylamide) and poly(N-isopropylmethacrylamide). J Phys Chem B 93:3311–3313

Gao J, Xu J, Wen S, Hu J, Liu H (2015) Plasma-assisted synthesis of Ag nanoparticles immobilized in mesoporous cellular foams and their catalytic properties for 4-nitrophenol reduction. Micropor Mesopor Mat 207:149–155

Jia L, Zhou F, Liu W (2012) Janus nanoparticle magic: selective asymmetric modification of Au-Ni nanoparticles for its controllable assembly onto attapulgite nanorods. Chem Commun 48:12112–12114

Khanna PK, Singh N, Kulkarni D, Deshmukh S, Charan S, Adhyapak PV (2007) Water based simple synthesis of redispersible silver nanoparticles. Mater Lett 61:3366–3370

Lee J, Jang DJ (2016) Highly efficient catalytic performances of eco-friendly grown silver nanoshells. J Phys Chem C 120:4130–4138

Lee J, Park JC, Song H (2008) A nanoreactor framework of a Au@$SiO_2$ yolk/shell structure for catalytic reduction of p-nitro-phenol. Adv Mater 20:1523–1528

Li D, He Q, Cui Y, Wang K, Zhang X, Li J (2007) Thermosensitive copolymer networks modify gold nanoparticles for nanocomposite entrapment. Chem Eur J 13:2224–2229

Li J, Liu J, Yang Y, Qin D (2015b) Bifunctional Ag@Pd-Ag nanocubes for highly sensitive monitoring of catalytic reactions by surface-enhanced Raman spectroscopy. J Am Chem Soc 137:7039–7042

Li W, Hua F, Yue J, Li J (2013) Ag@AgCl plasmon-induced sensitized ZnO particle for high-efficiency photocatalytic property under visible light. Appl Surf Sci 285:490–497

Li W, Yue X, Guo C, Lv J, Liu S, Zhang Y, Xu J (2015a) Synthesis and characterization of magnetically recyclable Ag nanoparticles immobilized on $Fe_3O_4$@C nanospheres with catalytic activity. Appl Surf Sci 335:23–28

Liu G, Wang D, Zhou F, Liu W (2015) Electrostatic self-assembly of Au nanoparticles onto thermosensitive magnetic core-shell microgels for thermally tunable and magnetically recyclable catalysis. Small 11:2807–2816

Liu G, Wang X, Zhou F, Liu W (2013) Core-shell-corona-structured polyelectrolyte brushes-grafting magnetic nanoparticles for water harvesting. ACS Appl Mater Interfaces 5:10842–11632

Liu L, Liu Z, Bai H, Sun DD (2012) Concurrent filtration and solar photocatalytic disinfection/degradation using high-performance Ag/$TiO_2$ nanofiber membrane. Water Res 46: 1101–1112

Liu Z, Yang C, Qiao C (2007) Biodegradation of p-nitrophenol and 4-chlorophenol by Stenotrophomona ssp. FEMS Microbiol Lett 277:150–156

Lu Y, Mei Y, Ballauff M, Drechsler M (2006) Thermosensitive core-shell particles as carrier systems for metallic nanoparticles. J Phys Chem B 110:3930–3937

Lu Z, Sun L, Nguyen K, Gao C, Yin Y (2011) Formation mechanism and size control in one-pot synthesis of mercapto-silica colloidal spheres. Langmuir 27:3372–3380

Matsuzaka N, Nakayama M, Takahashi H, Yamato M, Kikuchi A, Okano T (2013) Terminal-functionality effect of poly(N-isopropylacrylamide) brush surfaces on temperature-controlled cell adhesion/detachment. Biomacromolecules 14:3164–3171

Medasani B, Park YH, Vasiliev I (2007) Theoretical study of the surface energy, stress, and lattice contraction of silver nanoparticles. Phys Rev B 75:235436

Monteiro MJ, Cunningham MF (2012) Polymer nanoparticles via living radical polymerization in aqueous dispersions: design and applications. Macromolecules 45:4939–4957

Mu B, Zhang W, Wang A (2014) Facile fabrication of superparamagnetic coaxial gold/halloysite nanotubes/$Fe_3O_4$ nanocomposites with excellent catalytic property for 4-nitrophenol reduction. J Mater Sci 49:7181–7191

Naik B, Hazra S, Prasad VS, Ghosh NN (2011) Synthesis of Ag nanoparticles within the pores of SBA-15: an efficient catalyst for reduction of 4-nitrophenol. Catal Commun 12:1104–1108

Peng XH, Pan QM, Rempel GL (2008) Bimetallic dendrimer encapsulated nanoparticles as catalysts: a review of the research advances. Chem Soc Rev 37:1619–1628

Ravula S, Essner JB, La WA, Polo-Parada L, Kargupta R, Hull GJ, Sengupta S, Baker GA (2015) Sunlight-assisted route to antimicrobial plasmonic aminoclay catalysts. Nanoscale 7: 86–91

Sohrabnezhad S, Zanjanchi MA, Razavi M (2014) Plasmon-assisted degradation of methylene blue with Ag/AgCl/montmorillonite nanocomposite under visible light. Spectrochim Acta A 130:129–135

Sugiyama M, Salehi Z, Tokumura M, Kawase Y (2012) Photocatalytic degradation of p-nitrophenol by zinc oxide particles. Water Sci Technol 65:1882–1886

Sun L, Zhang R, Wang Y, Chen W (2014) Plasmonic Ag@AgCl nanotubes fabricated from copper nanowires as high-performance visible light photocatalyst. ACS Appl Mater Interfaces 6:14819–14826

Swathi T, Buvaneswari G (2008) Application of $NiCo_2O_4$ as a catalyst in the conversion of p-nitrophenol to p-aminophenol. Mater Lett 62:3900–3902

Tang Y, Jiang Z, Xing G, Li A, Kanhere PD, Zhang Y, Sum TC, Li S, Chen X, Dong Z, Chen Z (2013) Efficient Ag@AgCl cubic cage photocatalysts profit from ultrafast plasmon-induced electron transfer processes. Adv Funct Mater 23: 2932–2940

Uberoi V, Bhattacharya SK (1997) Toxicity and degradability of nitrophenols in anaerobic systems. Water Environ Res 69: 146–156

Wang MH, Fu JW, Huang DD, Zhang C, Xu Q (2013) Silver nanoparticles-decorated polyphosphazene nanotubes: synthesis and applications. Nanoscale 5:7913–7919

Wei H, Cheng SX, Zhang XZ, Zhuo RX (2009) Thermo-sensitive polymeric micelles based on poly(N-isopropylacrylamide) as drug carriers. Prog Polym Sci 34:893–910

Wu S, Dzubiella J, Kaiser J, Drechsler M, Guo X, Ballauff M, Lu Y (2012) Thermosensitive Au-PNIPA yolk-shell nanoparticles with tunable selectivity for catalysis. Angew Chem Int Ed 51:2229–2233

Xie Y, Yan B, Xu H, Chen J, Liu Q, Deng Y, Zeng H (2014) Highly regenerable mussel-inspired $Fe_3O_4$@polydopamine-Ag core-shell microspheres as catalyst and adsorbent for methylene blue removal. ACS Appl Mater Interfaces 6: 8845–8852

You YZ, Kalebaila KK, Brock SL, Oupický D (2008) Temperature-controlled uptake and release in PNIPAM-modified porous silica nanoparticles. Chem Mater 20:3354–3359

Zetterlund PB, Kagawa Y, Okubo M (2008) Controlled living radical polymerization in dispersed systems. Chem Rev 108:3747–3794

Zhang C, Li C, Chen Y, Zhang Y (2014) Synthesis and catalysis of Ag nanoparticles trapped into temperature-sensitive and conductive polymers. J Mater Sci 49:6872–6882

Zhang Z, Shao C, Sun Y, Mu J, Zhang M, Zhang P, Guo Z, Liang P, Wang C, Liu Y (2012) Tubular nanocomposite catalysts based on size-controlled and highly dispersed silver nanoparticles assembled on electrospun silica nanotubes for catalytic reduction of 4-nitrophenol. J Mater Chem 22:1387–1395

Zheng Y, Shu J, Wang Z (2015) AgCl@Ag composites with rough surfaces as bifunctional catalyst for the photooxidation and catalytic reduction of 4-nitrophenol. Mater Lett 158:339–342

Zhu M, Wang C, Meng D, Diao G (2013) In situ synthesis of silver nanostructures on magnetic $Fe_3O_4$@C core-shell nanocomposites and their application in catalytic reduction reactions. J Mater Chem A 1:2118–2125